Science Advances

AAAS

advances.sciencemag.org/cgi/content/full/3/3/e1600891/DC1

Supplementary Materials for

Extreme warmth and heat-stressed plankton in the tropics during the Paleocene-Eocene Thermal Maximum

Joost Frieling, Holger Gebhardt, Matthew Huber, Olabisi A. Adekeye, Samuel O. Akande, Gert-Jan Reichart, Jack J. Middelburg, Stefan Schouten, Appy Sluijs

Published 3 March 2017, *Sci. Adv.* **3**, e1600891 (2017)
DOI: 10.1126/sciadv.1600891

The PDF file includes:

- Supplementary Text
- fig. S1. Geological map of the Nigerian sector of the Dahomey Basin.
- fig. S2. Wall profiles for analyzed foraminifer species from the SQ.
- fig. S3. IB10A and IB10B TEX_{86} and BIT correlations.
- fig. S4. Environmental reconstructions for the IB10B core.
- fig. S5. Bayesian TEX_{86} calibrations using the IB10B data set and BAYSPAR tool (http://bayspar.geo.arizona.edu/) (*46*, *69*).
- fig. S6. IB10B chemostratigraphy and stratigraphical ranges of selected foraminifera and dinocysts.
- fig. S7. IB10A chemostratigraphy and stratigraphical ranges of selected foraminifera and dinocysts.
- fig. S8. Sensitivity plots for $\delta^{18}O_w$ and Mg/Ca_{sw}.
- table S1. Dinocyst assemblages for the Sagamu Quarry.
- table S2. Sea surface temperature (SST) data used in Figure 2D, E, G, H.
- References (*53–100*)

Other Supplementary Material for this manuscript includes the following:
(available at advances.sciencemag.org/cgi/content/full/3/3/e1600891/DC1)

- Data tables (Microsoft Excel format)

Supplementary Text

1. Biostratigraphy

Gebhardt et al. (*19*) identified planktonic foraminifer zones P4b to P5 and a negative carbon isotope excursion (CIE) in the planktonic foraminifer species *Morozovella acuta, Acarinina* spp. and benthic *Bulimina paleocenica* slightly above the P4c/P5 boundary in the Sagamu Quarry (SQ) section. They placed the P4/P5 boundary between 9.05 (sample #26) and 10.70 mbs (sample #28), based on the first occurrence of *M. subbotinae* at 10.70 m, rather than the last occurrence of a few damaged specimens of *Globanomalina pseudomenardii* at 10.70 m, which were interpreted to be bioturbated or reworked into younger sediments. The excursion taxa *Acarinina sibaiyensis* or *A. africana*, that mark planktonic foraminifer zone E1, are not recorded, likely because these index species appear during the peak of the PETM CIE (*53*) and only the start of the CIE is recorded at the Sagamu Quarry (*19*).

Samples for foraminifer stratigraphy In the IB10B core were taken prior to our sampling for a low-resolution study and are integrated over larger depth intervals and therefore not fully comparable with the depths in our isotope stratigraphy. Regardless, we find foraminifera indicative of planktonic foraminifer (sub-) zones P4b, P4c and P5 below 80 mbs (fig. S6). Crucially, we found no mixed-layer foraminifera in the peak of the CIE during examination of our new sample set. Exact stratigraphic positions of the late Paleocene foraminifer zones are hence difficult to constrain, but we record *G. pseudomenardii* from ~102 to 88 mbs, the first occurrence of *A. soldadoensis* at ~110 mbs and first occurrence of *M. subbotinae* around the onset of the CIE. We record *M. acuta,* (last occurrence 54.7 Ma (*31*)) from ~111-42 mbs (fig. S6).

The lower part (110-137 mbs) of the Oshosun FM in the IB10B core is marked by frequent occurrences of mixed Late Cretaceous and Early Paleocene foraminifera, suggesting significant reworking. However, dinocyst biostratigraphy provides complementary age constraints on this interval of the IB10B core. We record high abundances of *Apectodinium,* which regularly exceed the typical acme levels (>40%) recorded during the PETM in mid and higher latitudes (*54–57*). The genus has a (sub-) tropical affinity and has an oldest occurrence close to the Danian-Selandian boundary (*58*) in Egypt and Tunisia (*59*). The

unconformable surface between the Ewekoro limestones and the shales of the Oshosun formation (~140 mbs) must postdate the Danian-Selandian boundary based on the presence of *Apectodinium* in the Ewekoro limestones. We also find *Homotryblium* from the bottom of the Oshosun Fm. The oldest published occurrences of this genus are in the middle part of P4b (*59*, *60*). Combined with the foraminifer biostratigraphy, we find no evidence of sediments older than P4b in the lower part of the Oshosun Fm in the IB10B core.

2. Chemostratigraphy

The carbon isotope profile of the latest Paleocene of IB10B (Fig. 1B, fig. S6) is characterized by stable values of -25.2 ± 0.4 ‰. At 80 mbs, a first step in $\delta^{13}C_{TOC}$ of -1.2 ‰ occurs, followed by a short plateau stage and a second -2.8‰ step at 76.75 mbs again followed by a plateau stage until recovery starts at 70.75 mbs. The general $\delta^{13}C_{TOC}$ pattern is mimicked in the $\delta^{13}C$ of the palynological residue ($\delta^{13}C_{paly}$) that mostly consists of dinoflagellate cysts. However, $\delta^{13}C_{paly}$ values are up to ~7 ‰ higher than $\delta^{13}C_{TOC}$ in the interval between 80 and 77 mbs (Fig. 1B, fig. S6). This interval has relatively high TOC and extremely high dinocyst concentrations (Fig. 1D), suggesting high productivity. This likely skewed $\delta^{13}C_{paly}$ and $\delta^{13}C_{TOC}$ towards more positive values in this interval as high productivity leads to ^{13}C enrichment of dissolved inorganic carbon in the surface ocean. We therefore place the start of the CIE in the IB10B core at ~80 mbs. Based on the position of this CIE, directly above latest Paleocene foraminifer zones and below the last occurrence of *M. acuta*, we interpret this CIE to represent the PETM rather than any of the younger events in the Early Eocene such as Eocene Thermal Maximum 2, which occurred ~2 Ma after the PETM(*61*). The shape of this CIE, consisting of a steep decline, body and slow recovery provides additional support for this inference (*62–65*).

The isotope record of the IB10A core is very similar and given the presence of *G. pseudomenardii* in the same depth interval as in the IB10B core, we interpret the two low $\delta^{13}C_{TOC}$ values at 75-65mbs to represent the PETM (fig. S7).

3. Absolute temperature estimates

3.1 Mg/Ca temperature estimates

Mg/Ca was measured on glassy and hollow (fig. S2) planktonic *Acarinina spp*. and *Morozovella acuta*, and benthic *Bulimina paleocenica* and *Lenticulina olokuni*. We apply the calibrations of Anand et al. (*37*) and Lear et al. (*38*) for planktonic and benthic foraminifera, respectively, corrected for lower Paleocene seawater Mg/Ca ratios to calculate seawater temperature values.

$$T = (1/A)* \ln((Mg/Ca)_{test}/B)*[(Mg/Ca)_{sw}]^{H}/[(Mg/Ca)_{sw}']^{H}) \quad (1)$$

For planktonic foraminifera A = 0.085, B = 0.38 and for benthic foraminifera A = 0.109 and B = 0.867. Mg/Ca_{test} = foraminiferal test Mg/Ca Mg/Ca_{sw} = Mg/Ca ratio of modern seawater (5.15 mol mol^{-1}), Mg/Ca_{sw}' = Mg/Ca ratio of ancient seawater. We correct for the non-linear behavior of Mg/Ca_{test} under lower Mg/Ca_{sw} ratios by applying the equation of Evans and Muller (*36*) and use H = 0.42 following Dunkley Jones et al. (*4*). This value obtained for H is derived from cultured *G. sacculifer* and we note that 0.42 is the lowest observed values for H (*36*) in any modern genus and hence this may be considered a conservative estimate.

We assume a Paleocene Mg/Ca ratio of 2 mol mol^{-1} in line with recent estimates of Early Paleogene Mg/Ca ratios based on non-linear behavior of foraminifer Mg/Ca ratios under low ambient Mg/Ca (*36*). It should be noted that low ambient Mg/Ca increases uncertainties in high temperature environments (fig. S8B) and that previous studies use seawater Mg/Ca above or around 2 mol mol^{-1} (*4*, *59*, *60*). Furthermore, our reconstructed temperatures are outside the range of the respective calibrations for benthic and planktonic foraminifera. This means values are extrapolated and errors will be larger than the quoted calibration errors (1.13 °C; Anand et al. (*37*), 1.7 °C, Lear et al. (*38*)). Analytical errors are lower than 0.3 °C, which results in very conservative error estimates of ±1.4 and ±2 °C for planktonic and benthic foraminifera respectively.

3.2 $\delta^{18}O$ temperature estimates

We measured the same foraminifer species for $\delta^{18}O$ as for Mg/Ca. In order to reconstruct temperatures using the oxygen isotopes from foraminifer carbonate, several assumptions on local $\delta^{18}O_{sw}$ have to be made. First, we assume that no significant ice volume was present during the studied time period. The entire ocean would thus have been more depleted in $\delta^{18}O$ by approximately 1 ‰ (*68*). Secondly, several local or regional variations in $\delta^{18}O$ can bias the temperature estimates (*68*). The latitudinal effect on $\delta^{18}O_{sw}$ is fairly well known in modern open marine settings and can be approximated by applying a third order polynomial fit with latitude (x).

$$\delta^{18}O_{localsw} = 0.576 + 0.041x - 0.0017x^2 + 1.35*10^{-5}x^3 \quad (2)$$

We estimate paleolatitude, using the paleomagnetic reference frame of Torsvik et al. (*69*) and hotspot reference frame of Seton et al. (*15*) and arrive at a paleolatitude for our sites of ~1-7° S ((*16*); paleolatitude.org). To compare with models, which use the hotspot reference frame paleogeography, we use the 1 ºS estimate. Combining this with the ice volume effect, we arrive at an estimate of local $\delta^{18}O_w$ of -0.39 ‰. We consider this correction a crude estimate of the local $\delta^{18}O$, and it should be stressed that small changes in paleolatitude near the equator may strongly influence the local $\delta^{18}O_{sw}$.

Salinity fluctuations, which may occur in near shore settings and during periods of major hydrological change such as the PETM, typically lead to variations in $\delta^{18}O_{sw}$. From dinocyst assemblages we infer there are no significant salinity fluctuations that would impact $\delta^{18}O$. The majority of dinocyst species is of normal marine affinity, although some low-salinity tolerant species are present (Supplementary Table 1). Furthermore, symbiont-bearing planktonic foraminifera in the modern oceans are typically restricted to waters with salinity in excess of 34 and hence their presence suggests normal marine salinity (*70*). We also note that in case of enhanced fresh water supply, the tropical location would dampen the influence relative to a similar hydrological change at higher latitudes (*71*).

Furthermore, in high CO_2 environments, the concentration effect of the carbonate ion [CO_3^{2-}] on $\delta^{18}O$ is important and leads to decreased fractionation and hence underestimation of absolute temperatures (e.g. *62*). If a Paleocene pCO_2 of 1000 ppm is assumed, this results in a pH of 7.88 (pre-industrial 8.16) (*72*). The pH related decreased fractionation ranges from 0.89‰ for symbiont bearing foraminifera to 2.54‰ per pH unit for non-symbiont bearing foraminifera (*73*). This means that for the pH change relative to the modern, we may underestimate Paleocene absolute temperatures by 1 - 3.5 ºC. More importantly, pH changes during the PETM have a similar effect. pH is expected to decrease by about 0.25 unit (*74*), which could result in underestimated temperature change of 1 - 3 ºC. It is difficult to test whether the same pH effect holds on long time scales and long-extinct species. We hence use a conservative approach and only correct for the rapid pH change across the PETM in our data compilation. However, it should be noted that we likely underestimate absolute temperatures if the pH effect in Paleocene and Eocene species is similar to that of extant foraminifera.

We subsequently reconstruct temperatures by applying the equation from Kim & O'Neil (*39*) as used by Aze et al (*12*)

$$T = 16.1 - 4.64\,(\delta^{18}O_c - \delta^{18}O_w) + 0.09(\delta^{18}O_c - \delta^{18}O_w)^2 \quad (3)$$

In which $\delta^{18}O_c$ is the measured carbonate $\delta^{18}O$ and $\delta^{18}O_w$ is the local seawater $\delta^{18}O$. The equation of Kim & O'Neil (*39*) is calibrated for inorganic calcite, and the calibration is not limited to oceanic conditions or biotic limitations in foraminifera. The equation is continuous to at least 40 °C, with calibration and analytical errors of ±1.3 and ±0.3 °C respectively. This results in conservative error estimates for $\delta^{18}O$ of ±1.6 °C. Overall, sensitivity is lower for $\delta^{18}O_w$ and values are better constrained than past seawater Mg/Ca ratios (fig. S8).

3.3 TEX_{86} temperature estimates

Theoretically, TEX_{86} does not require any assumptions about water chemistry or past paleoenvironmental conditions, although some regions exhibit anomalous responses in the modern ocean (*33*). However, the isoprenoid glycerol dibiphytanyl glycerol tetraethers (GDGTs) used to calculate TEX_{86} are not exclusively biosynthesized by marine Thaumarchaeota. Methanogenic organisms living in organic rich sediments and methanotrophic organisms living in and near cold-seeps have been found to produce significant amounts of GDGTs. We apply the Methane Index of Zhang et al. (*25*) and GDGT ratios of Weijers et al. (*24*) and find that these never indicate significant GDGT input of methanotrophic or methanogenic Archaea (Supplementary Data).

TEX_{86} values may also be influenced by terrestrial input and therefore we calculate the relative abundance of terrestrially-derived branched versus marine isoprenoid GDGTs (BIT-index) (*23*), which typically uses a cut off value of 0.3 or 0.4 as limit for TEX_{86} data (*26, 27*). Most samples yield BIT values below 0.3 and we find no strong correlation between TEX_{86} and BIT (fig. S3). However, the topmost part (<50 mbs) of the IB10B core may have suffered from weathering and is associated with relatively high amounts of terrestrial lipids (BIT >0.5) a phenomenon typically observed in oxidized sediments (*75*). The high TEX_{86} values observed there may therefore be the result of a diagenetic bias.

Recently, debate has focused on GDGT distributions that are similar to modern Red Sea (*76*). The Red Sea GDGT distribution is notably different from open ocean GDGT distributions and has a different relation to temperature (*77*). These distributions are often characterized by high relative abundances of the crenarchaeol regioisomer (cren') (*76*), which is present in the original TEX_{86} equation. However, our samples do not show such an aberrant distribution during the latest Paleocene and PETM, as the relative abundance of cren' relative to that of cren averages ~10%. Hence, there is no direct potential for temperature overestimation due to Red Sea type Thaumarchaeota. We also find no indications of consistent basin restriction, strong stratification or high salinity in our dinocyst assemblages (fig. S4, supp. Data files). Assemblages mostly

comprise typical open marine species and although some proximal input is recorded, stratification indicators are rarely abundant.

3.4 TEX_{86} calibrations

Since the development of the proxy, several calibrations were proposed to calculate SST from TEX_{86} (see reviews of *71–73*). We consider several recent calibrations; TEX_{86}^{H}, TEX_{86}^{HC} (*33*) and the Bayesian TEX_{86} calibration (*35*) to retain clarity in this discussion. TEX_{86}^{H} is based on modern ocean core-top data and fits a logarithmic relation to SST. TEX_{86}^{HC} is also logarithmic, but calibrated with mesocosm cultures. Finally, Bayesian TEX_{86} calibration that aims to find similar TEX_{86} values from modern core-top data and fits a linear relationship.

TEX_{86}^{H} derived absolute temperatures agree well with carbonate proxy estimates of upper mixed-layer temperature (Fig. 1A). Our TEX_{86}^{H} values exceed the range of the core-top calibrated proxy. TEX_{86}^{HC} in contrast is based on mesocosm experiments, extending the upper temperature limit to 40 °C and potentially increasing the range by 10 °C. However, mesocosm studies of Thaumarchaea are limited and do not incorporate population differences and habitat depth, nor taphonomical effects such as diagenesis, burial, and transport, all of which are implicitly included in the core-top calibration.

The Bayesian TEX_{86} calibration is a promising new calibration, although this method is also highly sensitive to the non-modern-analogue setting reconstructed here. We use both the default settings to reconstruct temperature and a set of wider calibrations that incorporates most of the modern tropical and subtropical regions. The default setting, which applies search limits of 2 standard deviations (here 0.07 units) from the average TEX_{86} values yields temperatures typically 4 - 5 °C lower than carbonate based proxies. Crucially, however, in the default setting, the calibration utilizes one region from the modern ocean, the Red Sea. The Red Sea is a problematic region in the modern ocean with respect to $TEX_{86,}$ most likely because of a distinctly different population of Thaumarchaeota compared to the global ocean (*77*). The region is often

excluded from calibrations (*33*) because in this semi-enclosed basin, the relation between temperature and TEX_{86} is notably different than in the rest of the global ocean.

We stretched the Bayesian approach so that other high temperature tropical regions are incorporated (search limits 0.2, 0.15 and 0.135 TEX_{86} unit). These TEX_{86} calibrations generally yield values similar to those of the mesocosm studies. However, the relative influence of the Red Sea data is still important and reduces the reconstructed temperatures. It should be noted that the Bayesian TEX_{86} temperatures nearly always show a larger PETM warming, in the order of 4-5 °C rather than 2-3 °C derived from TEX_{86}^{H} and TEX_{86}^{HC}. Because we do not see any analogy between the Red Sea and the depositional setting of our analyzed sections in any ecological signal, geographical setting or GDGT profiles, we consider the validity of the Bayesian approach to be relatively low for this study.

Based on the convergence with carbonate-based proxies we prefer to use the core-top calibrated TEX_{86}^{H}, with the note of caution that, based on both the mesocosm calibrated TEX_{86}^{H} and the Bayesian calibrations covering modern tropical regions we may underestimate absolute temperatures. Confidence intervals of the Bayesian calibration suggest 90% confidence errors (±7 °C) may be larger than the combined analytical and core-top calibration error (90% confidence ±4.6 °C). It should be noted that this discrepancy is in part due to linear versus logarithmical approaches in the Bayesian TEX_{86} and TEX_{86}^{H}, respectively but notably due to incorporation of the Red Sea data in the Bayesian calibrations (fig. S5).

The production of GDGT lipids dominantly takes place in the top 300 m but also across the entire water column. However, it has been shown from sediment traps and surface sediments that generally only lipids produced in the upper 100 meters are effectively exported and deposited(*81*, *82*). Recent analyses have shown a substantial contribution of subsurface GDGTs to deep water sediments in the Mediterranean(*83*). Based on a statistical exercise and a number of assumptions, a recent paper has argued for a substantial contribution of subsurface GDGT to the TEX_{86} signal rather than only surface, on a global scale (*84*). Future contributions will undoubtedly test this hypothesis. Crucially, however, our sections and essentially all other

sections we use TEX_{86} data from are deposited on the continental shelf, excluding contributions of GDGTs produced in the deep ocean, implying that a SST calibration is appropriate here. Moreover, temperatures derived from $\delta^{18}O$ and Mg/Ca measured on planktonic foraminifera are in excellent agreement with TEX_{86}^{H} derived temperatures in the SQ. Therefore, we use TEX_{86}^{H} to reconstruct absolute SSTs in the SQ and the IB10B core.

4. Temperature change data compilation

For our data compilation of SST change across the PETM (hereafter referred to as ΔT), we use the data compilation of Dunkley Jones et al. (DJ2013 (*4*) and references therein) as a starting point. This compilation contains four different proxies for surface temperatures; $\delta^{18}O$, Mg/Ca, TEX_{86}^{H} and TEX_{86}'. Importantly, TEX_{86}' was only used to reconstruct pre-PETM temperatures from sediments from the Arctic Ocean (*2*, *85*). These sediments have very high BIT values, which implies that temperature estimates are likely less trustworthy, regardless of what calibration is used. We thus apply TEX_{86}^{H}, but only use sediments from the Arctic that have low BIT values, to retain consistency, and use earliest Eocene sediments as a substitute for latest Paleocene sediments to calculate ΔT. For all other data, we calculate ΔT from latest Paleocene and PETM sediments. It should be noted that difference between this approach and the previously published ΔT is not large. Reported ΔT of TEX_{86}' temperature is 3.9 ºC (*4*). In that case, the TEX_{86}' GDGT distribution was calibrated using the Kim et al. 2008 coretop dataset (*85*, *86*). Recalibrating TEX_{86}' with a log-transform calibration line and the Kim et al. 2010 coretop dataset (*33*) yields a ΔT of 3.4 ºC. TEX_{86}^{H} reconstructed temperatures are 2.9 ºC higher during the PETM compared to post PETM sediments.

A second important change to the DJ2013 data is a pH correction of 0.25 units (0.22‰) for all $\delta^{18}O$ estimates during the PETM. We only use symbiont-bearing foraminifera in our compilation and this increases all $\delta^{18}O$ derived ΔT by ~1 ºC.

We further add recently published data from several sections; the West Siberian Sea (*87*), North Sea area (*88*), Tanzania (*12*) and the South West Pacific (DSDP277) (*89*). We subsequently perform a bootstrap

(n=1000) approach on the data from each individual site to estimate mean ΔT and 5,25,50,75 and 95% quantiles of ΔT (Supplementary Table 2).

5. Plankton Regime Shift

Several hypotheses may be posed to explaining the demise in dinocyst abundances across the PETM in Nigeria. First, sediment accumulation rates increased at many marginal marine sites during the PETM due to hydrological change in the hinterland. However, the dinocyst abundance drop in the IB10B core cannot be explained by sedimentary dilution, as it requires an unrealistic increase in sediment accumulation to explain a three order of magnitude decrease ($10^5 > 10^2$ cysts/gram) in absolute dinocyst concentrations. Second, dinocysts may be subject to oxidation causing low concentrations in sediments. However, cysts of heterotrophic dinoflagellates, which are typically brown-pigmented, become a major part of assemblages during the PETM, although their absolute concentrations remain stable. Crucially, these brown-pigmented cysts are among the least resistant dinocysts (*90*), so their presence, as well as abundant benthic foraminifer linings, indicates optimal palynological preservation. We can therefore exclude oxidation as a cause of the dinocyst demise.

Third, we record isorenieratene and a diagenetic derivative throughout the onset and body of the CIE. This is a biomarker produced by photosynthetic green sulfur bacteria that need light and free sulfide, and therefore indicate the development photic zone euxinia (PZE) (*91*). This might have been toxic to dinoflagellates. However, other PETM records where PZE developed during the PETM (*87*, *92*, *93*) do not yield impoverished assemblages. Moreover, organic linings of benthic foraminifera increase in abundance during peak PETM (fig. S4D), suggesting at least intermittent water column oxygenation. In addition, redox sensitive trace metals indicate bottom waters experienced low oxygen conditions during the onset of the PETM (80-77 mbs), notably based on Mo and Cd enrichments (*94*), somewhat higher ratio values of organic C over total P (*95*) and the absence of benthic foraminifer linings (fig. S4). Clearly, however, this did not hinder dinocyst production. As the severity of anoxia and stratification appears to drop during the body of the CIE, we exclude anoxia/euxinia as a driver for the demise of dinoflagellates.

Fourth, massive freshwater influx from the continent may have caused salinities to drop below tolerance levels of many dinoflagellate species. Under such conditions, high abundances of dinocysts derived from low-salinity tolerant dinoflagellates would be expected in addition to the recorded species, as found in the Arctic Ocean (*92*) and New Jersey Shelf (*46*), even under low oxygen and euxinic water column conditions. However, we find no increase in such dinocyst species or fresh water palynomorphs, pollen and spores from terrestrial plants, or shifts in Ti/Al or Zr/Al that could indicate a dramatic increase in runoff and thereby a drop in salinity.

In our view, the most likely explanation for the demise of dinoflagellates is that conditions became too hot during the body of the PETM, when SSTs rose to values between 35°C and 37 °C. Such temperatures are uninhabitable for most eukaryotic organisms in the modern ocean because of enzymatic restrictions (*48*), even for dinoflagellates, which are among the most temperature resilient plankton groups (*49*). Some modern dinoflagellates produce heat-shock proteins, but these can only mediate short periods of thermal stress (*48*). Indeed, experiments have shown that temperatures above 35 °C are lethal to dinoflagellates, even while they reside in their cysts (*49*). Apart from often displaying narrow temperature tolerance ranges (*9*), many modern thermophilic organisms show a sharp decline in productivity and consequently survival when temperatures rise above optimum values.

Interestingly, the absolute concentration of brown-pigmented cysts appears more or less unaffected, leading to very high percentages (fig. S4F). These are, however, exclusively produced by heterotrophic dinoflagellates (*96*), which may well reside below the mixed layer. Collectively, we therefore attribute the recorded loss in dinoflagellate diversity and abundance to heat stress.

We recorded no mixed-layer dwelling foraminifera; only the thermocline dwelling *Subbotina* spp. are present in the IB10B body during the PETM. Although preservational biases in foraminifera are difficult to exclude, this may also result from heat-stress as previously suggested for the Indian Ocean (*12*).

Burial fluxes of benthic foraminifer linings peaked during the PETM, implying a retained production and flux of decent-quality organic matter to sustain benthic life. Given the known temperature tolerance of many extant eukaryotic primary producers, primary production was likely exclusively performed by prokaryotes in the study area at the reconstructed SSTs. Consistent with future projections, prokaryotes often outcompete eukaryotes under extreme conditions, including high temperatures (*97*). Cyanobacteria are the most likely candidates, since these often have high optimum growth temperatures (*50*) as well as high resistance against other common biological stress factors, e.g. UV radiation, high and low nutrients (*98*).

6. Dinoflagellate cysts ecology

We follow Sluijs et al. (*99*) for affinity of dinocyst species, unless indicated otherwise. Assemblages throughout the section are dominated by dinocysts of normal marine affinity and *Apectodinium*.

Normal Marine group

The "normal marine" group includes all genera and taxa that are thought to be representative of normal marine salinity, relatively low nutrient environments. There is considerable variance within this group, but only the shared normal marine affinity is important here. This group includes *Spiniferites*, *Achomosphaera*, *Hafniasphaera*, *Areoligera*, *Adnatosphaeridium*, *Glaphyrocysta* and the typically less abundant *Impagidinium* and *Operculodinium*. During the PETM, we find only *Spiniferites* spp., which is a generalist genus.

Apectodinium

All the species in the genus *Apectodinium* are considered of similar affinity. The genus is thought to be euryhaline, heterotrophic and therefore indicative of near shore, elevated nutrient conditions. The poleward migration of *Apectodinium* during the PETM and temperature-dependent appearance in the fossil record (*87*) suggests the genus had a fairly high minimum temperature requirement (20 °C) and occurred mostly in (sub-) tropical regions during the Late Paleocene and Early Eocene at temperatures over ~25 °C. The

assemblages during the Paleocene are dominated by aforementioned normal marine species and *Apectodinium* spp, which combined make up ~80% of the assemblage.

Low-salinity tolerant

This group includes *Senegalinium*, *Phthanoperidinium*, *Paleocystodinium*, *Lejeunecysta* and other Peridiniaceae with low relative abundances. Some of these, e.g. *Lejeunecysta* and *Paleocystodinium* are also brown-pigmented, as are modern strictly heterotrophic genera. *Senegalinium* and *Phthanoperidinium* were produced in large quantities in the Arctic Ocean when the sea surface was salinity was <5‰ during massive growth of the freshwater fern *Azolla* (*100*). We follow Sluijs and Brinkhuis (*46*), who considered all so-called 'hexa-peridinioids' to represent cysts of fresh-water tolerant dinoflagellates.

Protoperidinioids

The genera *Paleocystodinium*, *Lejeunecysta* and *Phelodinium* are primarily considered to represent cysts of heterotrophic dinoflagellates. *Lejeunecysta* and *Phelodinium*, are related to extant Protoperidinioid genera, which are almost exclusively heterotrophic. These cysts are usually considered to be least resistant to oxidation, relative to the normal marine, *Apectodinium* and low salinity tolerant cysts.

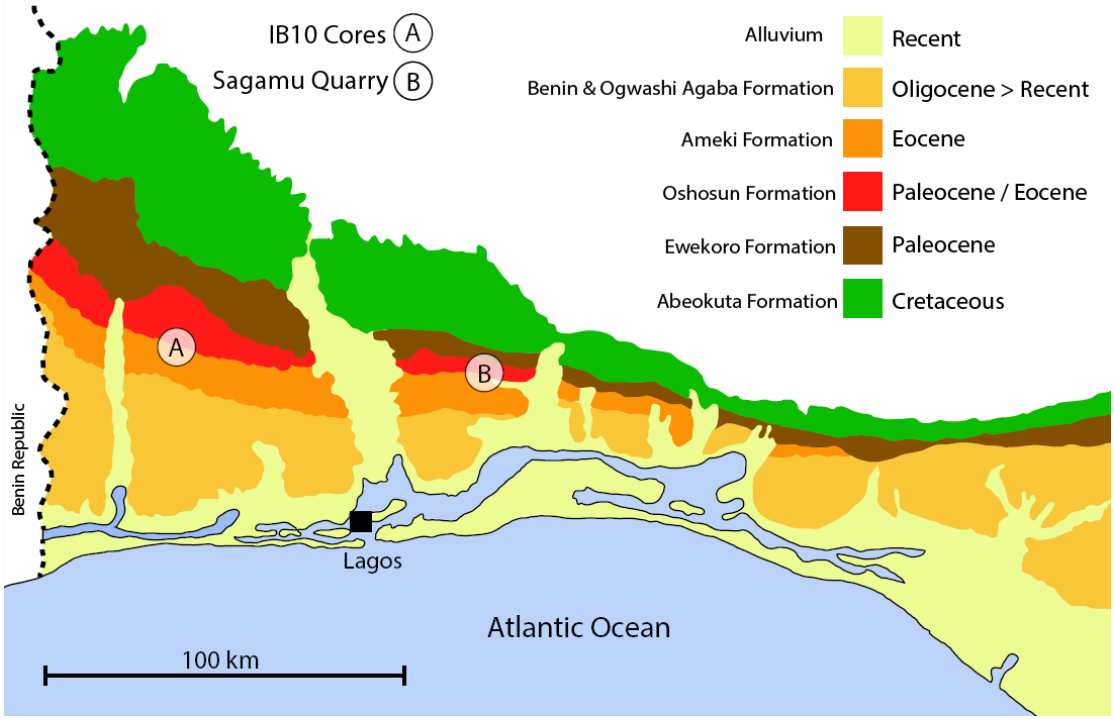

fig. S1. Geological map of the Nigerian sector of the Dahomey Basin. A; IB10 cores and B; Sagamu Quarry location.

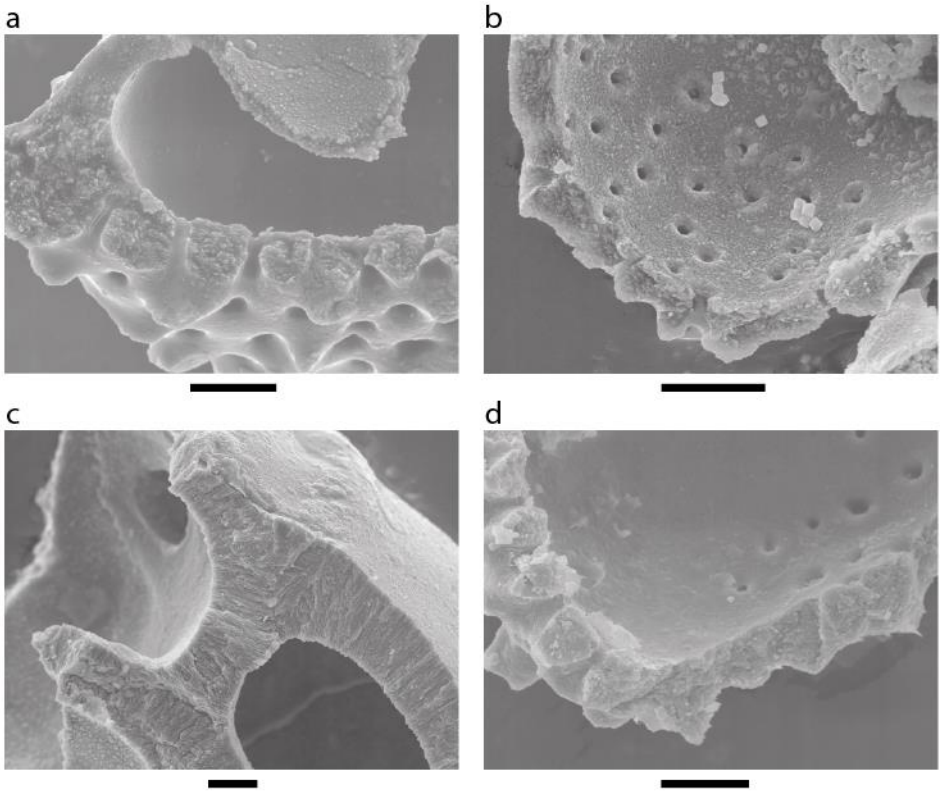

fig. S2. Wall profiles for analyzed foraminifer species from the SQ. A. *Morozovella acuta*. B. *Bulimina paleocenica* C. *Lenticulina olokuni* D. *Acarinina sp.* Scale bars, 10 μm.

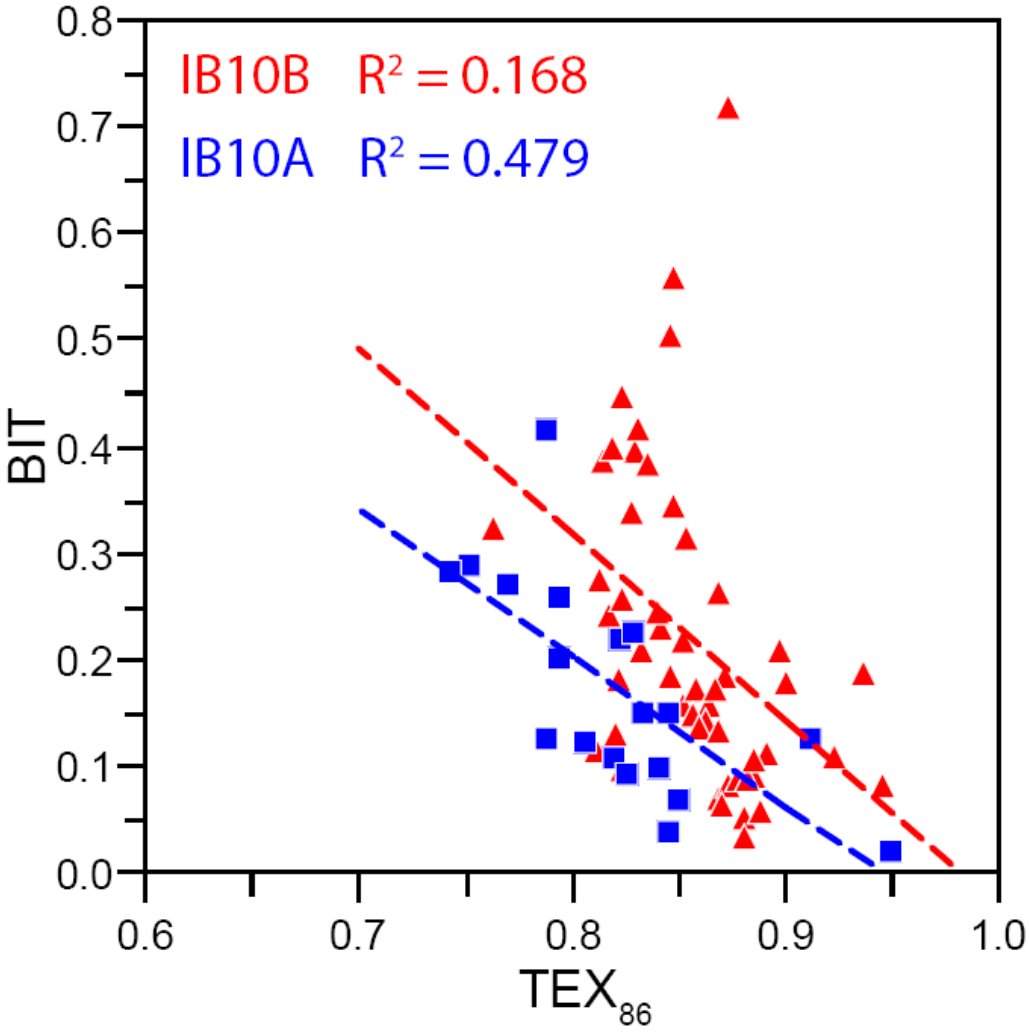

fig. S3. IB10A and IB10B TEX_{86} and BIT correlations. Note that a large part of the correlation is due to the high-TEX_{86}/low-BIT samples within the PETM interval.

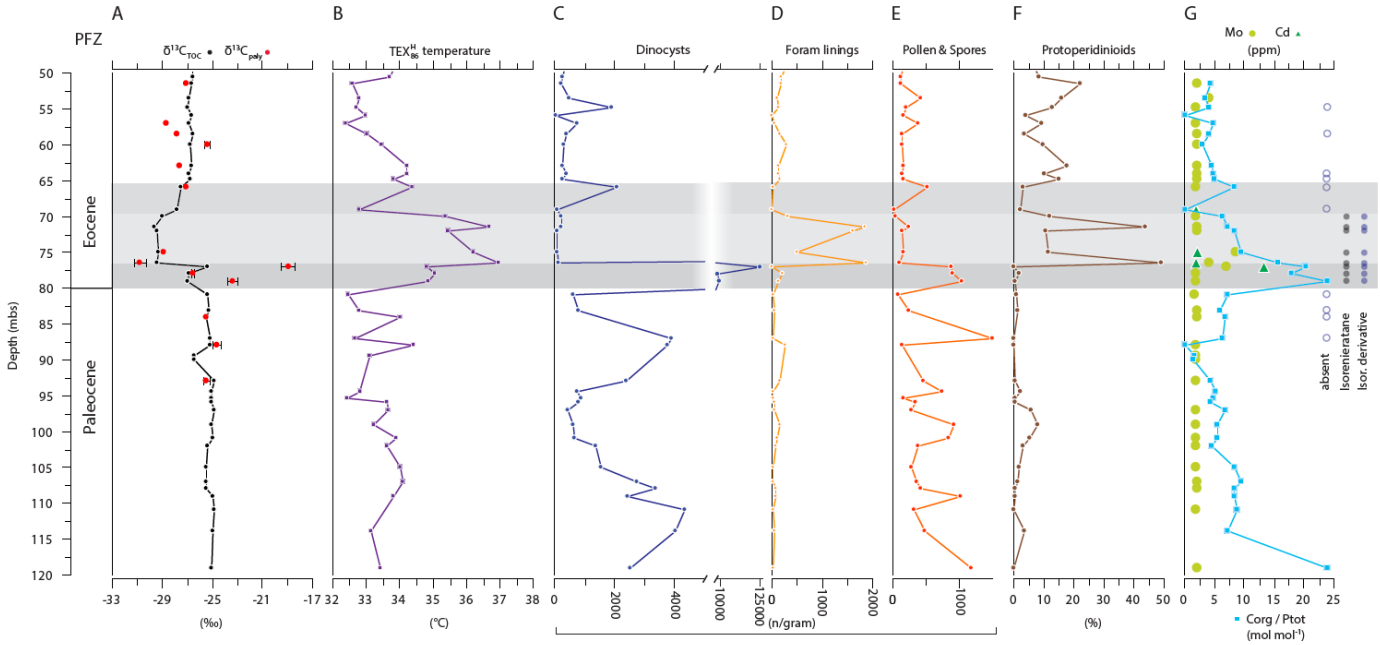

fig. S4. Environmental reconstructions for the IB10B core. A. Stable carbon isotope record of total organic carbon ($\delta^{13}C_{TOC}$) and palynological residue ($\delta^{13}C_{paly}$). **B.** TEX_{86}^{H} -based SST. **C.** Absolute concentrations of dinocysts per gram of dry sediment. Note the scale break at 4,000. **D.** Absolute concentration of organic foraminifera linings. **E.** Absolute concentration of pollen and spores. **F.** Relative abundance of Protoperidinioids. **G.** Indicators of anoxia: Organic carbon over total phosphorus ratio (Corg/Ptot) (light blue squares). Presence of isorenieratane and derivative. Concentrations of redox sensitive trace elements Mo (green circles) and Cd (blue circles) in ppm. Note that Mo concentrations are below the detection limit and absolute values should be treated with caution.

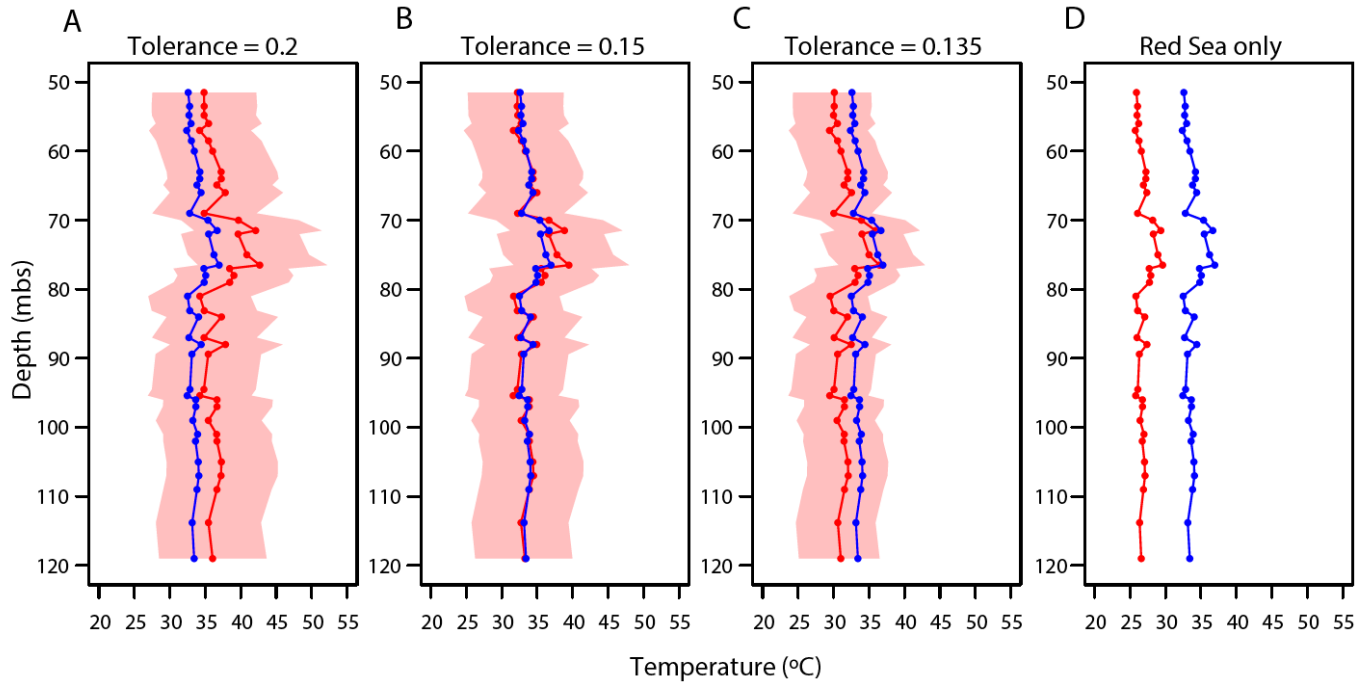

fig. S5. Bayesian TEX_{86} calibrations using the IB10B data set and BAYSPAR tool (http://bayspar.geo.arizona.edu/) (*46, 69*). The blue line is the standard TEX_{86}^{H} core top calibration, while the red lines and areas represent the Bayesian calibrations and 90% confidence intervals thereof. **A.** Calibration using all regions within 0.2 TEX_{86} units of data average. **B.** Similar, for 0.15 TEX_{86} units. **C.** Similar, for 0.135 TEX_{86} units. **D.** Red Sea (red line) calibration from Trommer et al. (*42*)

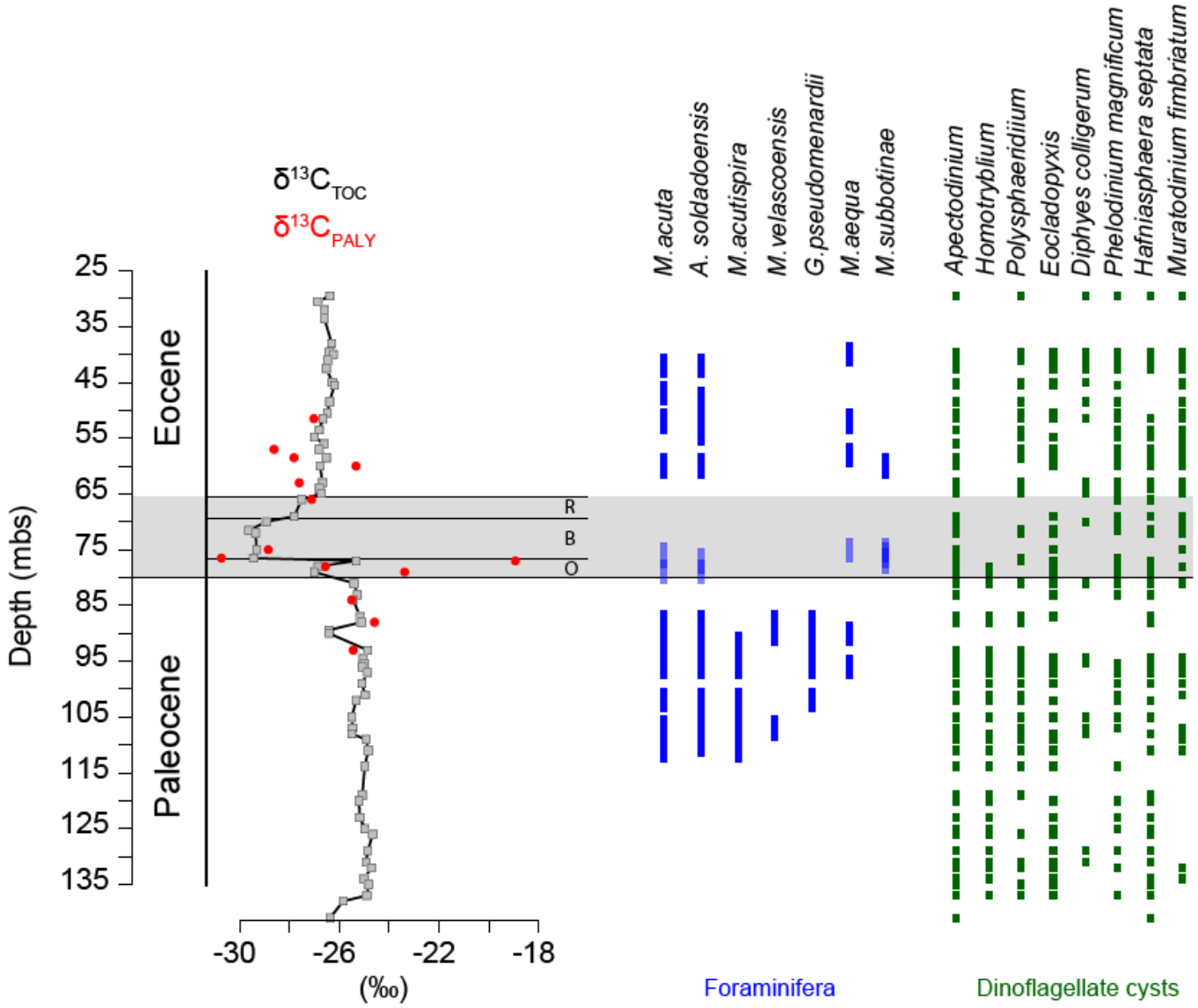

fig. S6. IB10B Chemostratigraphy and stratigraphical ranges of selected foraminifera and dinocysts. Stable carbon isotope records of total organic carbon ($\delta^{13}C_{TOC}$) in grey and palynological residue ($\delta^{13}C_{PALY}$) in red. Position of the CIE indicated (grey shaded area). Blue and green rectangles indicate presence of stratigraphically important foraminifera and dinocyst species. Note that foraminifer stratigraphy samples were taken for a low-resolution study; the samples are integrated over larger depth intervals and not fully comparable to depths of the isotope record. We found no mixed-layer foraminifera in the peak CIE during examination of the sample set analyzed for $\delta^{13}C$.

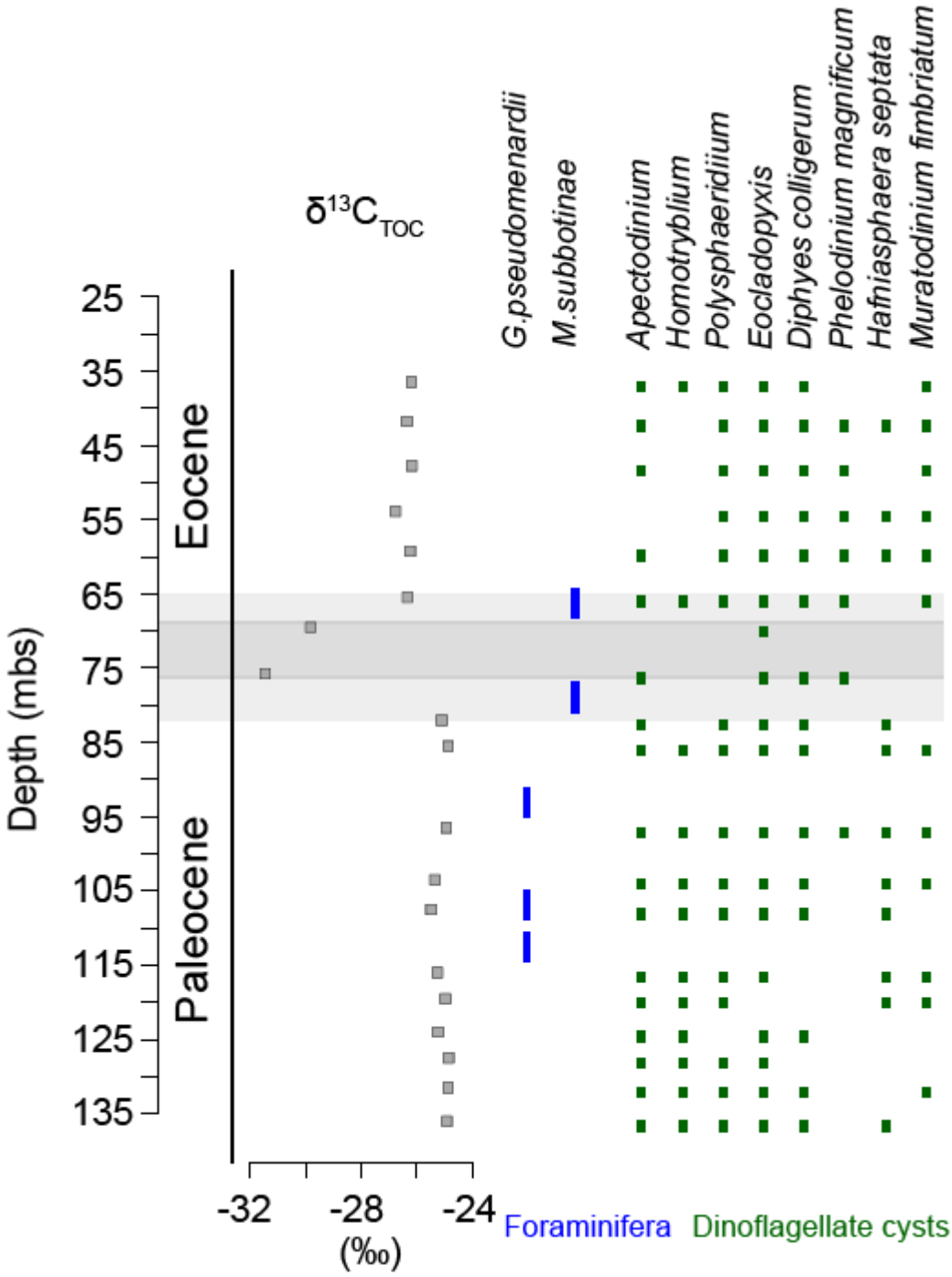

fig. S7. IB10A Chemostratigraphy and stratigraphical ranges of selected foraminifera and dinocysts. Stable carbon isotope records of total organic carbon ($\delta^{13}C_{TOC}$) in grey. Position of the CIE indicated (grey shaded area). Blue and green rectangles indicate presence of stratigraphically important foraminifera and dinocyst species.

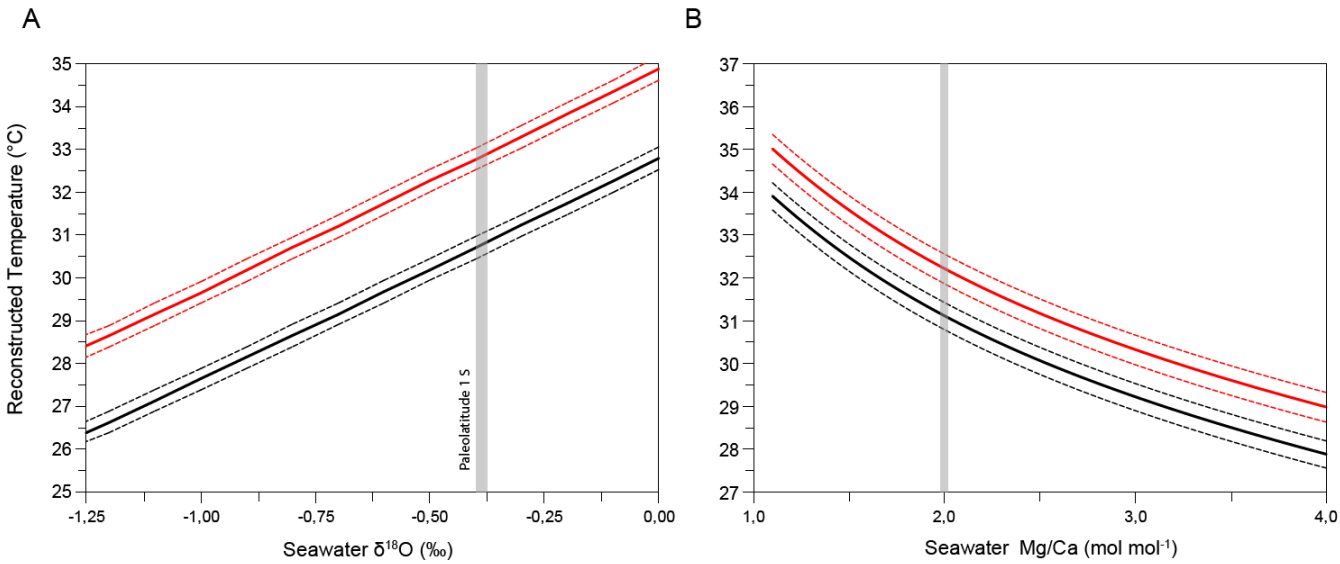

fig. S8. Sensitivity plots for $\delta^{18}O_w$ and Mg/Ca_{sw}. A. Sensitivity plot for $\delta^{18}O$-derived temperature against assumed local $\delta^{18}O_{sw}$. Solid lines indicate average *Morozovella acuta* (red) and *Acarinina sp.* (black), plus and minus analytical error (0.05‰) (dashed lines). **B.** Sensitivity plot for Mg/Ca seawater concentrations, solid and dashed lines same as above.

Sample	Depth (mbs)	Dinoflagellate assemblage (groups)													
		Apectodinium spp.	*Brown Peridinioids*	*Senegalinium spp.*	*Cerodinium/other P-cysts*	*Spiniferites cpx*	*Operculodinium*	*C. fibrospinosum cpx*	*Goniodomids*	*Areoligera cpx*	*Kallosphaeridium spp.*	*Impagidinium spp.*	*Diphyes spp.*	*Florentinia spp.*	*Proximate G-cysts*
SH27	9.80	41	0	0	1	35	2	2	3	0	11	0	2	3	0
SH25	11.60	13	0	0	0	52	0	3	1	0	27	0	0	1	0
SH23	13.20	33	0	1	2	38	3	4	5	2	9	0	0	1	1
SH21	14.10	40	1	1	7	32	0	0	3	0	10	0	0	3	4
SH19	14.80	26	1	2	1	50	1	2	2	0	7	0	0	2	4
SH18	15.10	22	2	2	1	37	1	0	8	0	12	0	0	5	6
SH16	16.00	32	1	1	3	42	1	2	1	0	6	0	0	1	7

Site	Paleolat	Paleolong	Palaeocene mean	lower 95%	upper 95%	PETM mean	lower 95%	upper 95%	deltaT	lower 95%	upper 95%	reported Palaeocene	reported PETM	delta T	0.25	median	0.75	Proxy	Reference
ACEX	83.2	31.3	18.2	17.8	18.6	22.9	22.5	23.1	4.6	4.1	5.1	18.6	22.4	3.9	4.4	4.6	4.8	TEX86'	Sluijs et al., 2006
	83.2	31.3	21.3	20.9	21.7	24.1	23.7	24.6	2.9	2.3	3.5				2.6	2.9	3.1	TEX86H	Sluijs et al., 2006
West Siberian Sea	54.6	66.0	18.3	17.3	19.4	27.2	26.8	27.7	8.9	7.5	10.1				8.4	9.0	9.5	TEX86H	Frieling et al., 2014
Denmark, Fur	52.5	4.1	19.6	17.3	22.0	29.8	28.6	30.9	10.1	7.0	13.0				8.9	10.2	11.6	TEX86H	Schoon et al. 2015
Denmark, Store Baelt	51.2	6.9	19.6	17.3	22.0	25.2	24.2	26.3	5.6	2.8	8.1				4.6	5.6	6.7	TEX86H	Schoon et al. 2015
Wilson Lake	38.2	-56.6	28.2	28.0	28.5	35.7	35.4	36.0	7.5	7.1	7.9	28.2	35.7	7.5	7.3	7.5	7.7	TEX86H	Zachos et al, 2006
Bass River	38.1	-56.1	23.4	22.5	24.2	27.7	27.1	28.3	4.3	3.2	5.4	23.2	26.2	3.0	3.8	4.2	4.7	*Acarinina* d18O	John et al., 2008
	38.1	-56.1	30.0	29.7	30.3	35.5	35.3	35.6	5.4	5.1	5.7	30.0	35.5	5.4	5.3	5.4	5.5	TEX86H	Sluijs et al. 2007
IODP1209	21.7	-157.9	29.4	29.2	29.5	33.2	32.8	33.6	3.9	3.5	4.3	29.4	33.2	3.9	3.7	3.8	4.0	*Acarinina* Mg/Ca	Zachos et al. 2003
	21.7	-157.9	29.6	29.5	29.8	33.6	33.3	33.8	3.9	3.6	4.2	29.6	33.6	3.9	3.8	3.9	4.1	*Morozovella* Mg/Ca	Zachos et al. 2003
	21.7	-157.9	20.6	20.2	21.0	22.6	22.2	22.9	2.0	1.4	2.5	20.4	21.2	0.8	1.7	2.0	2.2	*Acarinina* d18O	Zachos et al. 2003
	21.7	-157.9	20.8	20.0	21.5	23.9	23.7	24.1	3.1	2.3	3.9	20.6	22.5	1.9	2.8	3.0	3.4	Morozovella d18O	Zachos et al. 2003
ODP865	5.2	-143.5	31.1	30.2	32.0	33.2	32.3	34.0	2.1	0.9	3.3				1.6	2.1	2.6	Morozovella d18O	Kozdon et al. 2011
	5.2	-143.5	30.8	30.4	31.1	32.4	32.2	32.6	1.6	1.2	2.0	30.8	32.4	1.6	1.4	1.6	1.8	*Acarinina* Mg/Ca	Tripati & Elderfield, 2004
	5.2	-143.5	30.6	30.3	30.8	31.9	31.7	32.1	1.3	0.9	1.6	30.6	31.9	1.3	1.1	1.3	1.4	*Morozovella* Mg/Ca	Tripati & Elderfield, 2004
Nigeria (IB10B)	-0.7	-1.9	33.4	33.2	33.6	36.1	35.7	36.6	2.7	2.2	3.2				2.5	2.7	3.0	TEX86H	This study
Nigeria (IB10A)	-0.7	-1.9	32.7	32.2	33.1	36.5	35.9	37.1	3.8	3.0	4.6				3.4	3.8	4.2	TEX86H	This study
Tanzania	-19.0	33.7	30.5	30.1	31.1	35.4	33.3	37.4	4.9	2.8	7.0				4.0	4.9	5.8	*Morozovella* d18O	Aze et al., 2014
ODP527	-35.1	-8.1	16.1	15.9	16.4	20.4	20.2	20.8	4.3	3.9	4.7	16.6	19.8	3.1	4.1	4.3	4.5	*Acarinina* d18O	Thomas et al. 1999
	-35.1	-8.1	28.7	28.6	28.9	31.2	31.1	31.2	2.4	2.2	2.6	28.7	31.1	2.4	2.3	2.4	2.4	*Acarinina* Mg/Ca	Tripati & Elderfield, 2004
DSDP277	-62.7	-173.8	29.9	29.4	30.4	32.2	31.5	33.0	2.2	1.4	3.2				1.8	2.2	2.6	*Acarinina* Mg/Ca	Hollis et al. 2015
IODP1172	-64.8	160.2	25.9	25.8	26.1	31.8	31.3	32.3	5.9	5.4	6.4	25.9	31.8	5.9	5.7	5.9	6.1	TEX86H	Sluijs et al., 2011
ODP690	-65.2	-1.0	11.5	10.9	11.9	17.6	16.4	18.8	6.2	4.8	7.5	11.6	16.6	5.0	5.6	6.2	6.7	*Acarinina* d18O	Kennett & Stott, 1991
	-65.2	-1.0	10.8	10.5	11.2	21.2	21.0	21.5	10.4	10.0	10.8	11.1	20.0	9.0	10.2	10.4	10.6	*Acarinina* d18O	Thomas et al., 2002